SLAC–PUB–8456
May 2000

A Synchrotron-Light Interferometer for PEP-II*

Alan S. Fisher, Mark Petree and Eric L. Bong
Stanford Linear Accelerator Center, Stanford University, Stanford, CA 94309

Abstract

Transverse profile measurements in PEP-II, by imaging visible synchrotron emission from dipoles in the two rings, are broadened by surface errors on the primary extraction mirrors, due to the complex design to tolerate high beam currents. To improve vertical beam-size measurements, we recently installed a synchrotron-light interferometer, based on the concept of Mitsuhashi at KEK. In a two-slit interferometer, single-slit fringes are modulated by interference between the slits. Partial coherence decreases the modulation depth as the size of the emitting source increases, providing a sensitive measure of beam size. Because the slits pass light from two stripes along the mirror, we can select the better parts of the surface. In addition, segments of these stripes can be chosen by imaging the mirror onto the camera with a cylindrical lens, in the direction perpendicular to the fringe modulation. The interferometer is on the low-energy ring, 30 m from the *BABAR* detector, where the beam ellipse is tilted by 10º as we compensate for rotation in *BABAR*'s solenoid. Our design rotates the interferometer to measure the beam tilt. All optics are in the PEP tunnel and allow remote adjustment of the focusing, slit width and separation.

Talk presented at Beam Instrumentation Workshop 2000

Cambridge, Massachusetts, 8–11 May 2000

* Work supported by Department of Energy contract DE–AC03–76SF00515.

PEP-II STATUS

In the PEP-II *B* Factory at the Stanford Linear Accelerator Center [1], *B* mesons moving in the lab frame result from the collisions of 9-GeV electrons in the high-energy ring (HER) with 3.1-GeV positrons in the low-energy ring (LER). The first collisions were observed in July 1998. Immediately after the *BABAR* detector was installed in May 1999, we began commissioning the full system for several weeks. *BABAR* physics runs followed and have continued, with short interruptions, up to the time of this conference (May 2000). Table 1 shows a few design parameters [2], and Table 2 summarizes the machine's present performance. As the currents gradually increase, we remain on course toward achieving the design luminosity by the end of 2000; however, the specific (normalized) luminosity has been somewhat low. Since this parameter depends inversely on the overlapped *x* and *y* beam sizes at the interaction point (IP), we are interested in improving the accuracy of our beam-size measurements.

LIMITATIONS OF PEP'S SYNCHROTRON-LIGHT MONITORS

The synchrotron-light monitors (SLMs) for the PEP rings have been described previously [3]. In both, visible light reflected from two in-vacuum mirrors is imaged onto a CCD video camera. Our interest in adding a synchrotron-light interferometer was motivated by difficulties with each primary mirror (M1). The large beam current and consequent high heat load, plus the requirement for a low-impedance vacuum chamber, led to an M1 that is almost flush with the outer wall of the vacuum chamber and hit at grazing incidence. A 4-mm-high slot along the mirror's midplane passes the hot x-ray fan, while visible light reflects from the surfaces above and below. Because of grazing incidence, the x rays never reach the bottom of the slot, but travel past the mirror to dump their heat into a thermally separate absorber. Extensive water-cooling channels in M1 absorb the heat and prevent damage when the fan is not aligned with the slot.

TABLE 1. Some PEP-II Parameters.

Circumference [m]	2199.322
RF frequency [MHz]	476.399
Harmonic number	3492
HER energy [GeV]	8.97
LER energy [GeV]	3.12
CM energy [GeV]	10.58

The M1 mirrors for HER and LER were initially flat when polished, but once installed their images did not approach the diffraction limit. Subsequent investigation indicated that problems arose after polishing, when the long cooling tubes were welded to short tubing stumps on the rear surface. Further stresses

TABLE 2. PEP-II Status, May 2000.

Parameter	Typical	Achieved	Goal
HER current [mA]	600	900	750
LER current [mA]	1100	1750	2155
Number of full buckets	554	1658	1658
Luminosity [10^{33} $cm^{-2}\cdot s^{-1}$]	1.9	2.0	3.0
Specific luminosity [10^{30} $cm^{-2}\cdot s^{-1}\cdot mA^{-2}$]	2.0	2.6	3.1

appear to arise from the stiffness and weight of the tubes, and perhaps also from the mount holding the mirror in the vacuum chamber.

The PEP group has discussed building a new version of M1. However, a redesign is costly and still carries a risk of new problems. Instead, we have been pursuing a technique that has worked well at KEK in Japan, where various rings, including the KEK *B* Factory, now use the synchrotron-light interferometer developed by Toshiyuki Mitsuhashi [4]. One purpose of this paper is to make this work known to a wider audience. Also, we emphasize our adaptations to the needs of PEP, and particularly to the issue of M1 nonuniformity.

THE SYNCHROTRON-LIGHT INTERFEROMETER

When monochromatic light from a point source passes through a single slit, it forms the well known diffraction pattern with the $[(\sin x)/x]^2$ intensity. In Young's classic two-slit experiment, the light passing though parallel slits is combined on a screen. The two single-slit patterns interfere, creating a fine-scale modulation of the original envelope.

Now consider incoherent emission at a wavelength λ_0 from a large source *S*. The emitting points in *S* have uncorrelated phases, and so the fringes from different source points overlap and disappear. Between this case and the point source, there is a transition known as partial coherence, in which the modulation depth increases from 0 to 100%. In this régime, the modulation can be used to measure the source size. The general theory and history of partial coherence is developed in Born & Wolf [5]. Michelson originally used this technique to measure the angular diameter of stars.

To find the extent of this transition, consider the light at points P_1 and P_2 on the two slits. If over the entire source, the difference in path length is small,

$$\left|SP_1 - SP_2\right| \ll \lambda_0 , \tag{1}$$

then P_1 and P_2 remain correlated. This remains true for a source that is not strictly monochromatic, provided that this path difference is small compared to the coherence length for the bandwidth $\Delta\nu$:

$$c/\Delta\nu = \lambda_0^2/\Delta\lambda . \tag{2}$$

By inserting a narrow-band optical filter (in our case, a roughly Gaussian filter, centered at $\lambda_0 = 450$ nm and with a full width at half maximum of 30 nm), we can restrict ourselves to the case of quasi-monochromatic light. We also add a polarizer in front of the camera, to measure only the horizontally polarized light from the dipole, since the vertical component has a sign change at the midplane and therefore shifts the phase of its fringe pattern. Then we can apply the theorem of van Cittert and Zernicke [6], which shows that the expression for the fringe pattern is similar to a diffraction integral over the slits, but using the intensity rather than the electric field.

Consider a Gaussian electron or positron beam with an rms vertical size σ_y. (The measurement is one dimensional, and we have had more difficulty in measuring the smaller vertical size.) A distance s_0 away from the source is a pair of slits of width *a*

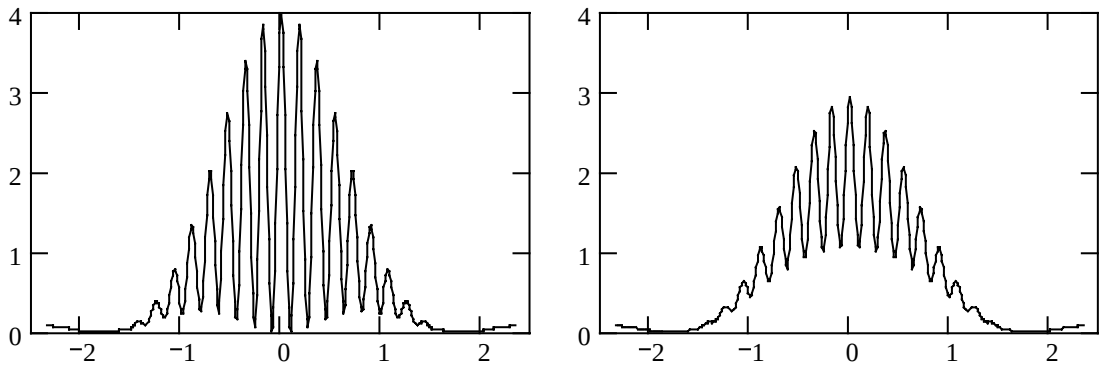

FIGURE 1. Calculated fringe intensity versus position (mm) on the CCD camera for (a) a point source and (b) a Gaussian with a 160-μm rms size. Other parameters, taken from PEP, are λ_0=450 nm, a 9.1-m distance from the source to the slits, and a 1.65-m focal length. The slit separation is 5 mm and the width is 0.5 mm. The fringes in (a) do not reach down to the axis because of the 30-nm width (FWHM) of the bandpass filter.

and center-to-center spacing *d*. The slit width is in the *y* direction and their length is in the *x* direction. They are symmetrically positioned at $y = \pm d/2$. The two single-slit diffraction patterns leaving each slit, as a function of the angle θ to the propagation axis *z*, are:

$$I_{\pm}(\theta) = A_{\pm}\left(\frac{\sin\left[\frac{ka}{2}\left(\theta \mp \frac{d}{2s_0}\right)\right]}{\frac{ka}{2}\left(\theta \mp \frac{d}{2s_0}\right)}\right)^2. \tag{3}$$

A short distance Δs away from the slits, a lens of focal length *f* directs the light to a screen (actually the CCD chip), at a distance $f + \Delta z$ beyond the lens. The optimal distance is the image plane, where the two single-slit patterns overlap:

$$\frac{1}{f + \Delta z_{\text{opt}}} = \frac{1}{f} - \frac{1}{s_0 + \Delta s}. \tag{4}$$

Now consider a point *y* on the screen. With the origin chosen at the center of the overall pattern, the relationship between the angle at the slit and the position on the screen is:

$$\theta_{\pm}(y) = \frac{y \pm \frac{d\Delta z}{2f}}{f + \Delta z\left(1 - \frac{\Delta s}{f}\right)}. \tag{5}$$

We now combine the light from the two slits and make use of the van-Cittert–Zernicke theorem to get the full expression for the fringe pattern:

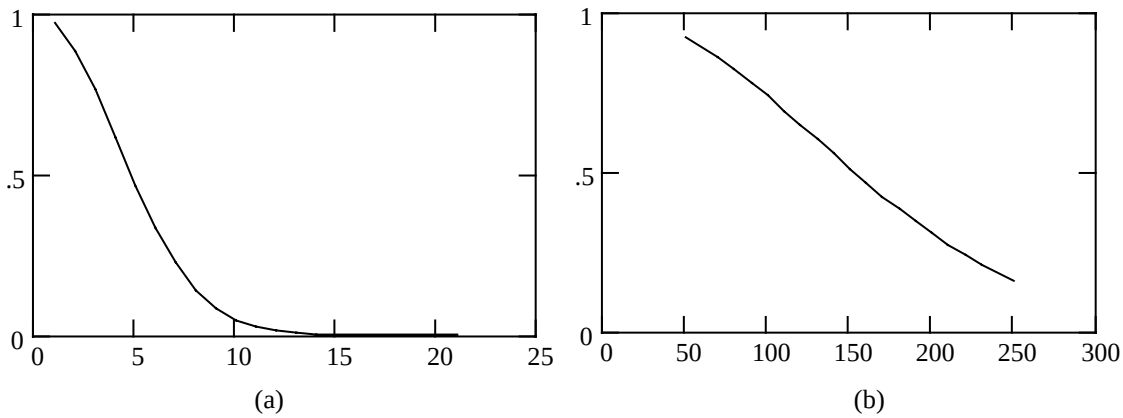

FIGURE 2. The variation of fringe visibility (modulation depth) with (a) the separation *d* of the slits, in mm; and (b) the rms height σ_y of the beam, in μm.

$$I(y) = \int_{-\infty}^{\infty} \left[I_+ + I_- + 2\sqrt{I_+ I_-} \exp\left(-\frac{(kd\sigma_y)^2}{2s_0^2} \right) \cos\left(\frac{kdy}{f + \Delta z} \right) \right] g(\lambda)\, d\lambda . \qquad (6)$$

Here we have integrated over the bandpass filter's normalized transmission $g(\lambda)$. The cosine factor in the third term gives the interference fringes, and the exponential shows their gradual disappearance with growth in beam size. When the intensity at the two slits is equal, and when the camera is on the image plane given by (4), then $I_+ = I_-$, and so (6) can be simplified. Fig. 1 illustrates this formula by showing the fringe patterns (a) for an ideal point source, $\sigma_y = 0$, and (b) for PEP's expected rms beam size of 160 μm.

The "visibility" of the fringes (modulation depth at the center of the pattern) is defined as:

$$V = \frac{I_{\max} - I_{\min}}{I_{\max} + I_{\min}} \qquad (7)$$

Fig. 2 shows the drop in visibility (a) as the slits get further apart and (b) as the beam size grows.

PEP'S INTERFEROMETER DESIGN

Imaging for M1 Compensation

The formulas above show that the interferometer can resolve beam sizes comparable to the 160-μm vertical size of the positron beam. Compared to direct imaging with our present SLM, the interferometer should also cope better with the distortion of M1. The mirror appears to be folded slightly along the midplane slot, and it has centimeter-scale irregularities where the cooling tubes attach. However, over much of its surface, the mirror is locally flat. Rather than using the entire surface, suitable optics let the interferometer select light from two portions of the surface.

The two slits transmit light from two narrow stripes along the mirror. When measuring the positron's vertical dimension, the slits and these stripes are parallel to *x*, selecting two *y* coordinates on the mirror. The fringe pattern consists of horizontal lines imposed on an image of the beam, as shown in Figure 3(a).

We can be more selective by imaging M1—rather than the source point—along *x*. A cylindrical lens, placed between the CCD and the spherical lens imaging the fringes, shortens the focal length along one axis and can image M1 onto the camera. Thus on the video screen, the *x* coordinates correspond to different *x* positions on the mirror, but the *y* coordinates still show the interference fringes. By digitizing the image and selecting the range of *x* with the clearest fringes, we have limited our use of M1 to two small rectangular zones.

Figure 3(b) shows such an image, achieved ten days before the start of this conference, when the full optical system was installed. The two vertical boundaries come from the left and right edges of M1. The fringes are much clearer than in Figure 3(a). They are also wavy rather than exactly parallel, which is a consequence of the distortion. In 3(a), without the cylindrical lens, the fringes from these different zones of M1 are blurred, reducing the contrast needed to extract the beam size.

Design Details

After M1, a second in-vacuum mirror sends the light through a window. A beamsplitter sends 5% of the light to the old imaging system. The remainder goes across the aisle to a 70-cm square box mounted on the wall. Depending on the position of a mirror on a motorized translation stage inside, the light can go either left to the interferometer or right along a 40-m path from the source to an optics hutch outside the shielding near *BABAR*. We use the hutch for streak-camera measurements. Between the window and the switching mirror, two steering mirrors with motorized tilts allow remote control of the beam direction for either path.

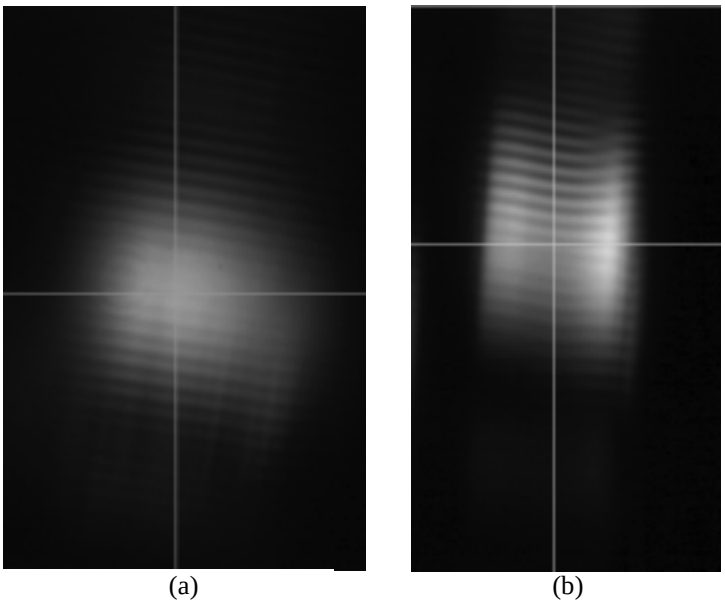

(a) (b)

FIGURE 3. Fringes from a beam imaged with (a) only the spherical lens, and (b) the cylindrical lens added. d = 7.8 mm, a = 0.8 mm. The slits have been rotated by (a) 10º and (b) 5º from having their long axes aligned with the beam's horizontal. The boundaries in (b) on the left and right are images of the sides of mirror M1.

The interferometer is also on the tunnel wall, in a 3-m box adjacent to the box with the switching mirror. The interferometer was kept close to the source to avoid the expense of the many large-diameter mirrors needed for a diverging beam, and to avoid

any consequent wavefront distortion. (The streak-camera path uses four lenses to relay the image, but wavefront quality is less of a consideration for this application. The first lens, on the shared path to both the streak camera and the interferometer, is removed by another motorized translation stage when the interferometer is in use.)

The interferometer slits are sandwiched between a pair of 15-cm square optical breadboards. The inner and outer jaws, made with razor blades, form two pairs that move together. The inner jaws are mounted on the lower plate on a pair of small translation stages moving in opposite directions, perpendicular to the axis. One motor driving a third stage separates the jaws by driving a wedge plate between them. The outer jaws, which hang from the upper plate, are mounted and driven similarly. A fold of black paper, which expands as the jaws separate, blocks the space between the inner jaws. The spherical lens follows the jaws on the lower breadboard.

The positrons' beam ellipse rotates in passing through the *BABAR* solenoid, 30 m away from the synchrotron-light source point. To compensate, a series of skew quadrupoles starting in the upstream arc pre-tilts the beam before it reaches *BABAR*, so that it levels out when reaching the IP. A similar series of skew quads removes the tilt that accumulates in the second half of *BABAR*, so that the beam is properly decoupled through the rest of the ring. The synchrotron source point is half way through the downstream skew-quad sequence; if the skew quads are adjusted ideally, the major axis of the beam should be tilted there by 10º. Because the ellipse is not upright, and because we want to measure its size along the minor axis, the entire interferometer breadboard assembly is mounted on a motorized rotation stage with a range of 120º.

The CCD camera is 2 m away in the same interferometer enclosure. The camera rides on a 150-mm translation stage to focus the fringes as the beam orbit varies. A narrow-band (30 nm FWHM) image-quality optical filter and polarizer are also on the stage, just in front of the camera. The polarizer is oriented to transmit light polarized in the bend plane of the emitting dipole magnet. This orientation is somewhat complex because here the positrons do not follow a straight line parallel to the tunnel axis; instead, they are in the middle of a gradual 90-cm rise from the height of the electrons in *BABAR* to the height they maintain in the rest of the ring. They are also at an angle horizontally as they return from being brought into collision by horizontal bends. The mirrors that transport the light are carefully placed to avoid mixing the two polarizations from the source while still aligning them at the interferometer with the horizontal and vertical axes relative to the tunnel wall.

The cylindrical lens, between the primary (spherical) lens and the camera, must rotate with the slit assembly, to always focus in the orthogonal plane to the fringe pattern. It is coupled to the downstream side of the rotation stage with a meter-long pair of concentric tubes. To focus on M1, we can't move the camera, since its position is determined in the other plane, for best focus on the source. Instead, we have another 150-mm translation stage moving the cylindrical lens. Because the lens must rotate too, the coupling tubes telescope to allow translation, but lock together to allow rotation. The weight of the downstream section is supported from the translation stage by bearings near the cylindrical lens.

Data Acquisition

The images are acquired by a monochrome, analog CCD (Pulnix TM7-EX), which includes an electronic "shutter" that gates the chip for intensity control. The images are then digitized just outside the shielding by a PCI-bus frame-grabber in a PC running Windows NT 4.0. Control of the acquisition and data analysis uses software based on LabView, a widely used system combining a graphical interface with a graphical way of controlling instruments, manipulating images, and performing mathematical routines. We also use Beam Analysis, a commercial package of LabView routines for analyzing Gaussian beams (developed for the laser industry), so that much of the work of image acquisition and presentation was done for us. The power of this approach is that the full LabView code is provided (as VI routines), and so it is relatively straightforward to supplement the package with routines specific to fringe analysis. We have adapted LabView's nonlinear curve-fit routine to find the various parameters in the fringe equations (3) through (6), especially the beam size. We still must add LabView code to rotate the image (to undo the rotation of the slits), select a rectangular region where the image of M1 provides the sharpest fringes, project these fringes onto the axis, and supply this curve to the curve-fit routine.

Next this information must be supplied to the PEP control system, which is an integrated combination of the older SCP system developed for SLAC's linear collider (SLC), and EPICS for newer devices. The SCP runs under VMS on a DEC/Compaq Alpha, and uses mouse clicks on buttons drawn in a text window, along with displays in a graphics window. EPICS is a Unix-based graphical interface supported by a consortium of accelerator laboratories. In particular, the Los Alamos EPICS group has developed an EPICS "channel access" interface that allows LabView routines on a PC to communicate with EPICS computers as if the PC were just another EPICS machine reading and writing values for EPICS variables ("channels"). With this feature, our LabView code will be able to pass results seamlessly to our existing control software. We can then log data in our history buffers, prepare strip charts on a control screen, or use the SCP's correlation-plot software, which can step one or two controls (magnets, for example, or a simple time sequence) while measuring the effect on up to 160 diagnostic channels.

The final issue we are now beginning to address is remote viewing and control of the images and user interface on the LabView screen. The raw images are transported to the control room, roughly 500 m away, by cable TV, but the user must be able to control the program in order to select the region of interest on the image. We are now testing a freeware program called VNC, which combines a server on the computer you want to control with a "viewer" program on a remote computer, which shows the screen of the server and allows full mouse and keyboard control. Versions are available for Windows, Macintosh, VMS and Unix. An alternative is a commercial program like PC Anywhere, but these all require that both machines run Windows. It may also be possible for the PC to drive an X window directly in the control room.

ACKNOWLEDGMENTS

We wish to thank Toshiyuki Mitsuhashi and John Flanagan of KEK for their helpful discussions and their tour of the KEKB optics. As always, we appreciate the efforts of our many colleagues at SLAC, and at the Lawrence Berkeley and Lawrence Livermore National Laboratories, who have made PEP-II so successful.

REFERENCES

1. Supported by U.S. Dept. of Energy contract DE-AC03-76SF00515.
2. *PEP-II: An Asymmetric* B *Factory*, Conceptual Design Report, LBL-PUB-5379, SLAC-418, CALT-68-1869, UCRL-IC-114055, UC-IIRPA-93-01, June 1993.
3. Fisher, A.S., "Instrumentation and Diagnostics for PEP-II," *Proc. Beam Instrumentation Workshop*, Stanford, CA, 4-7 May 1998, AIP Conf. Proc. **451** (Amer. Inst. Phys., Woodbury, NY, 1998), pp. 395-403.
4. Mitsuhashi, T., "Beam Profile and Size Measurement by SR Interferometers," in *Beam Measurement*, Proc. Joint US-CERN-Japan-Russia School on Particle Accelerators, Montreux, Switzerland, 11-20 May 1998 (World Scientific, Singapore), pp. 399-427.
5. Born, M., and Wolf, E., *Principles of Optics*, 5th ed. (Pergamon Press, Oxford, 1975).
6. *ibid.*